Available online at www.sciencedirect.com

ScienceDirect

Nuclear Physics B 899 (2015) 180–193

NUCLEAR PHYSICS B

www.elsevier.com/locate/nuclphysb

# Higgs effects in top anti-top production near threshold in $e^+e^-$ annihilation

M. Beneke [a], A. Maier [a,*], J. Piclum [b], T. Rauh [a]

[a] *Physik Department T31, James-Franck-Straße 1, Technische Universität München, 85748 Garching, Germany*
[b] *Albert Einstein Center for Fundamental Physics, Institute for Theoretical Physics, Sidlerstrasse 5, CH-3012 Bern, Switzerland*

Received 7 July 2015; accepted 30 July 2015

Available online 6 August 2015

Editor: Tommy Ohlsson

**Abstract**

The completion of the third-order QCD corrections to the inclusive top-pair production cross section near threshold demonstrates that the strong dynamics is under control at the few percent level. In this paper we consider the effects of the Higgs boson on the cross section and, for the first time, combine the third-order QCD result with the third-order P-wave, the leading QED and the leading non-resonant contributions. We study the size of the different effects and investigate the sensitivity of the cross section to variations of the top-quark Yukawa coupling due to possible new physics effects.


## 1. Introduction

Top anti-top quark production near threshold in $e^+e^-$ collisions provides a unique opportunity to measure the top-quark mass precisely, due to the well-defined center-of-mass energy and the enhancement of the cross section due to the strong-interaction Coulomb force. Whether the required theoretical precision on the cross section can be achieved has been an open question, since the second order (non-relativistic) QCD calculations revealed unexpectedly large corrections and uncertainties [1,2]. After many years of work, the third-order QCD calculation has been

* Corresponding author.
*E-mail address:* a.maier@tum.de (A. Maier).

http://dx.doi.org/10.1016/j.nuclphysb.2015.07.034

recently finished [3], resulting in a largely reduced theoretical uncertainty. With QCD effects under control, the emphasis shifts to other effects which must be addressed for a realistic cross section prediction. The most important are Higgs effects associated with the top-quark Yukawa coupling, general electromagnetic and electroweak corrections, non-resonant production of the final state $W^+W^-b\bar{b}$ in the center-of-mass region near twice the top-quark mass, $2m_t$, and photon initial-state radiation.

In this paper, we mainly focus on Higgs-boson effects and the sensitivity to the top-quark Yukawa coupling. The Yukawa potential generated by Higgs exchange [4], one-loop Higgs corrections to $t\bar{t}$ production [5], and both together [6] have been considered long ago, but these early calculations do not reach the precision that corresponds to the third-order QCD calculation in the non-relativistic power-counting scheme. Third-order Higgs corrections to the production vertex and the energy and wave-function at the origin of a hypothetical S-wave toponium resonance have been computed in [7], but the $t\bar{t}$ cross section has not yet been considered. We supply this missing piece here. We also add for the first time the P-wave contributions [8] and the leading non-resonant contributions [9,10] to the third-order S-wave QCD calculation. We then allow the top-quark Yukawa coupling $y_t$ to deviate from the Standard Model relation[1] $m_t = y_t v/\sqrt{2}$ and investigate the sensitivity to such deviations given the current theoretical uncertainties.

## 2. Higgs effects at NNNLO

The contribution of the Higgs boson to the top pair production cross section $e^+e^- \to t\bar{t}$ introduces two new parameters, the Higgs mass $m_H$, and top-quark Yukawa coupling $y_t$. To set up the calculation we have to fix their relation to $m_t$ and the strong and electroweak couplings, $\alpha_s$ and $\alpha_{\rm EW}$, to establish the power counting. Recall that it is customary to count $\alpha_s \sim v$ and $\alpha_{\rm EW} \sim \alpha_s^2$, where $v = [(\sqrt{s} - 2m_t)/m_t]^{1/2}$ is the small top-quark velocity. A contribution of order $\alpha_s^k$ (or, equivalently, $v^k$) according to this counting is called "N$^k$LO" or "$k$th order". We opt for counting $y_t^2 \sim \alpha_{\rm EW} \sim \alpha_s^2$ and $m_H \sim m_t$. Other options would be to count the top–Yukawa coupling like the strong coupling, $y_t^2 \sim \alpha_s$, or the Higgs mass $m_H \sim m_t v$, or both. Clearly, with $m_t \approx 173$ GeV, $m_H \approx 125$ GeV and $v \sim 1/10$, the counting $m_H \sim m_t$ is more appropriate. In the terminology of non-relativistic effective theory and the threshold expansion, the Higgs mass is of order of the hard scale, and not the potential scale, which has significant impact on the structure of the contributions. On the other hand, the counting of the coupling simply determines at which orders in the expansion the Higgs contributions appear and we will justify our choice below.

The effective field theory setup is described in detail in [11]. We recall that the dominant S-wave production cross section is proportional to the imaginary part of the spectral function of the vector current

$$\Pi^{(v)}(q^2) = \frac{3}{2m_t^2} c_v^2 G(E) + \ldots, \tag{2.1}$$

where $c_v$ is the hard matching coefficient of the vector current, $E = \sqrt{s} - 2m_t$, and $G(E)$ is the Green function in potential-nonrelativistic QCD (PNRQCD), i.e. the propagator of a non-relativistic top anti-top pair. The Higgs contributions to $c_v$ are discussed in Section 2.1. To compute the corrections to the Green function the Higgs contributions to the PNRQCD Lagrangian

[1] The symbol $v$ is used for the Higgs vacuum expectation value and the top-quark velocity, see below. The meaning should be clear from the context.

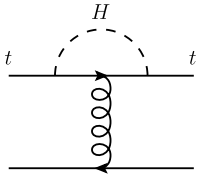


Fig. 1. One-loop Higgs correction to the color Coulomb potential.

have to be determined. Counting $m_H \sim m_t$ implies that the Yukawa-potential $\exp(-m_H r)/r$ generated by Higgs exchange between the top quarks is replaced by the local interaction $\delta^{(3)}(\mathbf{r})/m_H^2$ as is apparent from the Higgs propagator $1/(\mathbf{q}^2 + m_H^2)$ in momentum space, where $\mathbf{q}^2 \sim m_t^2 v^2$ can be neglected (expanded) relative to $m_H^2$. On the other hand, with $m_H \sim m_t v$, both terms would have to be kept. The contribution to the momentum-space potential is therefore simply

$$\delta_H V = -\frac{y_t^2}{2m_H^2}. \tag{2.2}$$

We note that this is suppressed by $v^3$ with respect to the leading QCD Coulomb potential $\alpha_s/\mathbf{q}^2$, where one power of $v$ arises from the counting of the Yukawa coupling, and two powers from the relative factor $\mathbf{q}^2/m_H^2$. The Higgs-induced potential is thus a NNNLO effect. The corresponding correction to the Green function $G(E)$ is computed in Section 2.2.

Furthermore we have to consider corrections to the color Coulomb potential as shown in Fig. 1. With $m_H \sim m_t$ counting, only the hard loop momentum region can yield a contribution. Since the external momenta are potential they have to be expanded, and we are left with an $\mathcal{O}(y_t^2)$ zero-momentum transfer correction to the $\psi^\dagger \psi A^0$ top-quark–gluon coupling of the NRQCD Lagrangian. However, since the top field is renormalized in the on-shell scheme this contribution cancels.

### 2.1. Short-distance effects

With $y_t \sim \alpha_s$ the leading, one-loop Higgs contribution to the hard matching coefficient of the vector current is of second order. It has been computed in [5,12,13]. Due to an additional diagram involving a $ZZH$ vertex, the matching coefficients for the $\gamma t\bar{t}$ and the vector part of the $Zt\bar{t}$ vertex differ. We neglect the contribution from this diagram and use the $\gamma t\bar{t}$ coefficient, since the difference amounts to less than one percent of the already small NNLO Higgs contribution to the production vertex [5]. At NNNLO there are mixed Higgs and QCD corrections to the vector current. They have been computed as expansions for $m_H \approx m_t$ or $m_H \gg m_t$ in [7], which is consistent with the adopted hard $m_H \sim m_t$ scaling. We use the result expanded in $(1 - m_t^2/m_H^2)$, which was denoted $1b$ in [7] and was shown to converge quickly for Higgs boson masses around the physical value of about 125 GeV. Based on the results of [7] we estimate the truncation error due to this expansion to be well below one percent of the NNNLO matching coefficient and neglect it in the following. The NNNLO correction to the hard matching contains an IR divergence, which can be absorbed into a renormalization constant for the vector current

$$\widetilde{Z}_v = 1 + \big[\text{pure QCD}\big] + \frac{\alpha_s C_F}{4\pi}\frac{y_t^2 m_t^2}{2m_H^2}\frac{1}{4\epsilon}. \tag{2.3}$$

The renormalized hard matching coefficient for the vector current can be parametrized by

$$c_v = 1 + \big[\text{pure QCD}\big] + \frac{y_t^2}{2}\left[c_{vH}^{(2)} + \frac{\alpha_s}{4\pi}c_{vH}^{(3)}\right] + \ldots, \tag{2.4}$$

where $c_{vH}^{(i)}$ can be obtained from [7]. For convenience we reproduce the relevant expressions in Appendix A. The pure QCD correction is also known to NNNLO [14]. Starting at NNLO there is also a self-energy correction to the Z boson mediated cross section that contains the Higgs boson. Since it does not involve the top Yukawa coupling we do not consider it here. It will be added together with other NNLO electroweak and non-resonant effects in future work.

To justify the power counting $y_t \sim \alpha_s$ we compare the size of the Higgs effects discussed above to their QCD counterparts. For the hard matching coefficient we obtain, with $\alpha_s(\mu = 80\ \text{GeV}) = 0.1209$,

$$c_v = 1 - 0.103|_{\alpha_s} - 0.022|_{\alpha_s^2} + 0.031|_{y_t^2} - 0.070|_{\alpha_s^3} - 0.019|_{y_t^2\alpha_s} + \ldots, \tag{2.5}$$

where the contributions from different orders of the couplings are shown explicitly. The power counting is clearly valid here. For the potentials it is natural to compare the Higgs potential (2.2) to the spin-projected QCD NNLO Darwin potential $\delta V_D$, which is also local. Adopting $\alpha_s$ from above, we find $\delta_H V = -0.98/m_t^2$, which is only slightly smaller than $\delta V_D = 8\pi\alpha_s C_F/(3m_t^2) = 1.35/m_t^2$. However, since the Darwin potential yields only a small correction compared to other NNLO effects we conclude that the overall counting is appropriate.

### 2.2. Potential contributions

The potential correction to the Green function can be obtained by quantum mechanical (PNRQCD) perturbation theory due to the instantaneous, hence particle number conserving nature of potentials. Since the Higgs potential (2.2) is a NNNLO effect, only the single insertion of $\delta_H V$ is required to compute the NNNLO correction to the Green function

$$\delta_H G(E) = \langle \mathbf{0}|\hat{G}_0(E)\, i\delta_H V\, i\hat{G}_0(E)|\mathbf{0}\rangle = -\delta_H V\, G_0(E)^2. \tag{2.6}$$

The remarkably simple form arises because of the locality of the potential. The Green function $G_0(E)$ describes the propagation of a top quark pair, produced and destroyed at zero spatial separation, under the influence of the leading-order QCD Coulomb potential. The insertion of a local interaction thus factorizes into the product of a Green function to the left and the right of the insertion. Using the well-known result for the LO Green function

$$G_0(E) = \frac{m_t^2\alpha_s C_F}{4\pi}\left[\frac{1}{4\epsilon} + L_\lambda + \frac{1}{2} - \frac{1}{2\lambda} - \hat{\psi}(1-\lambda) + \mathcal{O}(\epsilon)\right], \tag{2.7}$$

in $d = 4 - 2\epsilon$ space–time dimensions, expressed through $\lambda = \alpha_s C_F/(2\sqrt{-E/m_t})$, $L_\lambda = \log(\lambda\mu/(m_t\alpha_s C_F))$, and $\hat{\psi}(x) = \gamma_E + \psi(x)$, we observe that the imaginary part of (2.6) is UV divergent,

$$\text{Im}\,[\delta_H G(E)]|_{\text{div}} = \frac{y_t^2}{m_H^2}\frac{m_t^2\alpha_s C_F}{16\pi\epsilon}\,\text{Im}\,[G_0(E)], \tag{2.8}$$

where $G_0(E)$ denotes the exact $d$-dimensional LO Green function. Note that this expression also contains a finite term from the $1/\epsilon$ pole multiplying the unknown $\mathcal{O}(\epsilon)$ part of the LO Green function. However, (2.8) exactly cancels in the combination $\text{Im}[(c_v\widetilde{Z}_v^{-1})^2 G(E)]$. This is

analogous to the cancellation between the divergent part of the QCD Darwin potential single insertion and part of the divergence of the two-loop QCD contribution to $c_v$. In the following, we therefore only have to consider the finite part

$$\delta_H G_{\rm fin}(E) = \frac{y_t^2}{2m_H^2}\left(\frac{m_t^2\alpha_s C_F}{4\pi}\left[L_\lambda + \frac{1}{2} - \frac{1}{2\lambda} - \hat\psi(1-\lambda)\right]\right)^2. \tag{2.9}$$

Due to the non-perturbative treatment of the LO Coulomb potential in PNRQCD, the exact Green function contains single poles below threshold, which correspond to ${}^3S_1$ toponium bound states:

$$G(E) \stackrel{E\to E_n}{\longrightarrow} \frac{|\psi_n(0)|^2}{E_n - E - i\epsilon}. \tag{2.10}$$

The energy levels $E_n$ and squared wave functions at the origin, $|\psi_n(0)|^2$, also receive corrections from the insertion of the Higgs potential. We use the parametrization

$$\begin{aligned} E_n &= E_n^{(0)}\left(1 + [\text{pure QCD}] + \frac{\alpha_s}{4\pi}\frac{y_t^2}{2} e_H\right), \\ |\psi_n(0)|^2 &= |\psi_n^{(0)}(0)|^2\left(1 + [\text{pure QCD}] + \frac{\alpha_s}{4\pi}\frac{y_t^2}{2} f_H\right), \end{aligned} \tag{2.11}$$

where

$$E_n^{(0)} = -m_t\left(\frac{\alpha_s C_F}{2n}\right)^2, \qquad |\psi_n^{(0)}(0)|^2 = \frac{1}{\pi}\left(\frac{m_t\alpha_s C_F}{2n}\right)^3. \tag{2.12}$$

The corrections $e_H$, $f_H$ can be obtained by expanding (2.9) and (2.10) around the bound-state energies and comparing coefficients. Alternatively both equations can be expanded around positive integer values of $\lambda$. For (2.9) we obtain

$$\delta_H G_{\rm fin}(E) = \frac{y_t^2}{2m_H^2}\frac{m_t^4\alpha_s^2 C_F^2}{16\pi^2}\left[\frac{1}{(n-\lambda)^2} + \frac{2}{n-\lambda}\left(L_n + \frac{1}{2} - \frac{1}{2n} - \hat\psi(n)\right) + \ldots\right], \tag{2.13}$$

where $L_n = \log(n\mu/(m_t\alpha_s C_F))$ and the ellipsis denotes terms that are regular in the limit $\lambda \to n$. We obtain

$$e_H = \frac{m_t^2 C_F}{m_H^2}\frac{2}{n}, \qquad f_H = \frac{m_t^2 C_F}{m_H^2}\left(2L_n + 1 + \frac{4}{n} - 2S_1(n)\right). \tag{2.14}$$

Here $S_1(n) = \sum_{k=1}^n k^{-1}$ denotes the harmonic number of order one. The result for $e_H$ agrees with [7] and for $f_H$ we reproduce the value for $n = 1$ given in [7].

### 2.3. Combined

Combining hard and potential effects due to the Higgs boson, more precisely, the top–Yukawa interaction with the Higgs boson, we can express the NNLO correction to the vector correlation function (2.1) as

$$\delta_{2H}\Pi^{(v)} = \frac{3}{2m_t^2} y_t^2 c_{vH}^{(2)} G_0(E). \tag{2.15}$$

The NNNLO correction is

$$\delta_{3H}\Pi^{(v)} = \frac{3}{2m_t^2}\left[\frac{\alpha_s}{4\pi}y_t^2(c_{vH}^{(3)} + c_{vH}^{(2)}c_1)G_0(E) + y_t^2 c_{vH}^{(2)}\delta_1 G(E) + \delta_H G_{\rm fin}(E)\right]. \qquad (2.16)$$

It includes cross terms of the NNLO Higgs correction with the known NLO QCD corrections to the Green function, $G(E) = G_0(E) + \delta_1 G(E) + \ldots$, and matching coefficient $c_v = 1 + \alpha_s c_1/(4\pi) + \ldots$. Both terms are finite, as it is understood here that $G_0(E)$ from (2.7) is minimally subtracted. The physical cross section is related to the imaginary part of $\Pi^{(v)}(q^2)$.

## 3. Non-resonant and QED effects

In the computation of QCD and Higgs corrections to the $t\bar{t}$ cross section the top decay width has been accounted for by the replacement $E \to E + i\Gamma_t$, where both quantities are of the same order. Since the top quark is unstable, one should rather consider the production cross section for the decay product $W^+W^-b\bar{b}$ of the top pair.[2] This final state can also be produced without an intermediate resonant top pair and only the sum of both processes constitutes a physical quantity. This is also apparent from an incomplete cancellation of UV divergences and scale dependence in the non-relativistic description of the resonant process starting at NNLO. The non-resonant correction is important for realistic cross section predictions, since it affects particularly the cross section below the position of the peak, where the sensitivity to the top-quark mass is largest [3].

The computation of the $e^+e^- \to W^+W^-b\bar{b}$ cross section in the top anti-top threshold region, such that it is consistent with the non-relativistic power counting, expansion and resummation of the resonant sub-process, can be performed in the framework of unstable-particle effective theory [15,16]. The master formula for the cross section is

$$\begin{aligned} i\mathcal{A} = &\sum_{k,l} C_p^{(k)} C_p^{(l)} \int d^4x\, \langle e^-e^+|\mathrm{T}[i\mathcal{O}_p^{(k)\dagger}(0)\, i\mathcal{O}_p^{(l)}(x)]|e^-e^+\rangle \\ &+ \sum_k C_{4e}^{(k)} \langle e^-e^+|i\mathcal{O}_{4e}^{(k)}(0)|e^-e^+\rangle. \end{aligned} \qquad (3.1)$$

The first line describes the resonant production of the $t\bar{t}$ pair through an operator $\mathcal{O}_p^{(k)}$. Since the initial state is color-neutral, the matrix element further factorizes into a leptonic and a hadronic tensor as long as only QCD and no electroweak effects are considered, and the non-relativistic treatment in terms of the PNRQCD Green function $G(E)$ is recovered. The second line describes non-resonant production of the $W^+W^-b\bar{b}$ final state, which is why the hadronic contribution can be absorbed fully into a hard Wilson coefficient. The leading non-resonant effects appear already at NLO in the non-relativistic power counting, and have been determined in [9], including the possibility of imposing invariant-mass cuts on the top decay products. The result for the total cross section was confirmed in [10] with an independent method. In the following analysis we combine the results from [9] with the third-order QCD calculation [3]. We exclude the small contribution from $e^+e^- \to W^+W^-H$ followed by $H \to b\bar{b}$, since it can be considered as a reducible "background" and eliminated by an invariant-mass cut on the $b\bar{b}$ jets as discussed in [9]. At NNLO only partial results for the non-resonant term in the second line of (3.1) are available [10,17,18]. We do not consider them here and hope to include the complete NNLO non-resonant correction together with other NNLO electroweak effects in future work. We note

[2] The W boson can be treated as stable here, since its kinematics is not sensitive to the W width.

that the cancellation of divergences at NNLO has already been demonstrated [17] and that the contribution is likely to be numerically relevant below threshold.

There is, however, one further electroweak effect already at NLO. The counting $\alpha \sim \alpha_s^2$ of the QED coupling implies that the QED Coulomb potential $\delta V_{\rm QED} = -4\pi\alpha Q_t^2/\mathbf{q}^2$ represents a NLO correction relative to the leading order QCD Coulomb potential. While only a single insertion of this potential would be required for NLO accuracy, we include contributions involving the NLO QED Coulomb potential up to NNNLO, i.e. we also include multiple insertions of $\delta V_{\rm QED}$ as well as mixed insertions together with other potentials and current matching coefficients. The required expressions can be inferred from the known results for multiple insertions of the QCD potentials [19,20], but one has to be careful when considering insertions which contain divergences in the imaginary part, since the QCD Coulomb potential contains $\mathcal{O}(\epsilon)$ terms which are absent in the QED potential. The QED potential has already been included in previous calculations [9,21,22], but not yet in combination with the third-order QCD result [3]. Similarly, the numerical effect of the NLO non-resonant terms was studied in detail in [9], but was not implemented so far in the code that includes the higher-order QCD corrections.

## 4. Size of Higgs and other non-QCD effects

For the cross section predictions shown below we employ the values

$$m_t^{\rm PS}(20\ {\rm GeV}) = 171.5\ {\rm GeV}, \quad \Gamma_t = 1.33\ {\rm GeV} \tag{4.1}$$

for the top-quark PS mass [23] and top-quark width. We note that the QED Coulomb potential is not part of the definition of the PS mass, since, in contrast to QCD, higher-order QED corrections do not give rise to an IR renormalon ambiguity in the pole mass, and are rapidly decreasing. The strong and electromagnetic couplings are

$$\alpha_s(M_Z) = 0.1185 \pm 0.006, \quad \alpha(M_Z) = 1/128.944, \tag{4.2}$$

where the QCD coupling refers to the $\overline{\rm MS}$ scheme and the running QED coupling, taken from [24], to the on-shell scheme. These parameters are taken to be consistent with [3]. We further use

$$M_W = 80.385\ {\rm GeV}, \quad M_Z = 91.1876\ {\rm GeV}, \quad m_H = 125\ {\rm GeV} \tag{4.3}$$

for the electroweak gauge and Higgs boson masses, from which we derive the Weinberg angle, Higgs expectation value $v$ and top–Yukawa coupling $y_t = \sqrt{2}m_t/v$ through tree-level relations. Here $m_t$ is the top pole mass, computed from the PS mass with NNNLO accuracy.

The QCD NNNLO result includes the P-wave contribution at the same order, computed in [8], which arises from production of the $t\bar{t}$ pair through the axial-vector coupling of a virtual $Z$-boson. This enhances the $S$-wave cross section presented in [3] by about 1%. The theoretical uncertainty of the cross section calculation itself is estimated by varying the renormalization scale between 50 and 350 GeV. The "default scale" is set to 80 GeV. The "finite-width" factorization scale $\mu_w$ related to the separation of resonant and non-resonant terms in (3.1) is fixed to $\mu_w = 350$ GeV. The dependence on this scale is canceled exactly order-by-order in the sum of the two contributions. Since presently the non-resonant terms are included only to NLO, while the resonant terms are known to NNNLO, there is a small uncanceled dependence on $\mu_w$ at NNLO.

In Fig. 2 we show the total $e^+e^- \to W^+W^-b\bar{b}$ cross section in the range of $e^+e^-$ center-of-mass energy $\sqrt{s}$ a few GeV below and above the top anti-top threshold including the Higgs, QED and non-resonant corrections discussed above (red/dark-grey hatched band) and compare it to the QCD-only result at NNNLO (light-grey hatched band). The cross section is

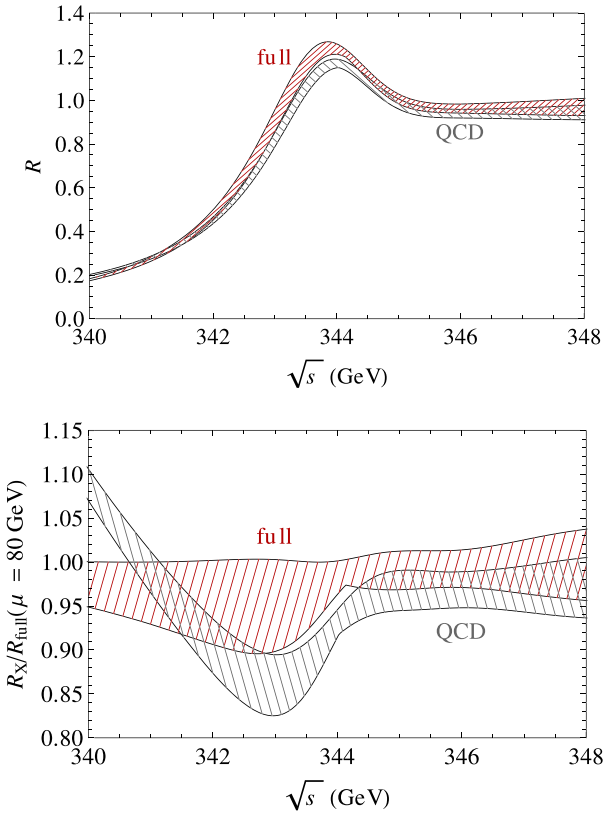


Fig. 2. The $R$ ratio for QCD-only (light-grey hatched band) and including the Higgs, QED, and non-resonant contributions (red/dark-grey hatched band) as functions of the center-of-mass energy. The bands are due to the scale variation. The upper plot shows the absolute results and the lower plot the results normalized to the full one evaluated at the scale $\mu = 80$ GeV. (For interpretation of the references to color in this figure legend, the reader is referred to the web version of this article.)

always normalized to the LO cross section for $e^+e^- \to \mu^+\mu^-$, yielding the so-called $R$ ratio $R = \sigma(e^+e^- \to W^+W^-b\bar{b})/\sigma_0$, with $\sigma_0 = 4\pi\alpha^2/(3s)$. The QED and Higgs potentials lead to an attractive force, which enhances the cross section. The leading Higgs contribution to the short-distance coefficient (2.5) is also positive, resulting in an overall enhancement of about 10% near and 5% above the peak. Below the peak the negative non-resonant contribution becomes important and wins over the QED and Higgs enhancement. The lower plot in Fig. 2 contains the same results as the upper one, but now all values have been normalized to the full $R$ ratio evaluated for $\mu = 80$ GeV. Comparing the two bands, we again observe the enhancement of the full cross section around and above the peak. The rise in the QCD-only result at energies below the peak is due to the non-resonant contribution, which decreases the full cross section in this region. We observe a small increase in the scale uncertainty of the full result relative to QCD-only, which can now reach $\pm 5\%$ about one GeV below the peak, but is mostly of the $\pm 3\%$ size. The additional scale dependence arises mainly from the Higgs potential insertion.

The size of the three non-QCD contributions considered here — the Higgs, QED and non-resonant contributions — are shown separately in Fig. 3, normalized to the NNNLO QCD-only result for the total $t\bar{t}$ cross section and plotted as function of the $e^+e^-$ center-of-mass energy $\sqrt{s}$

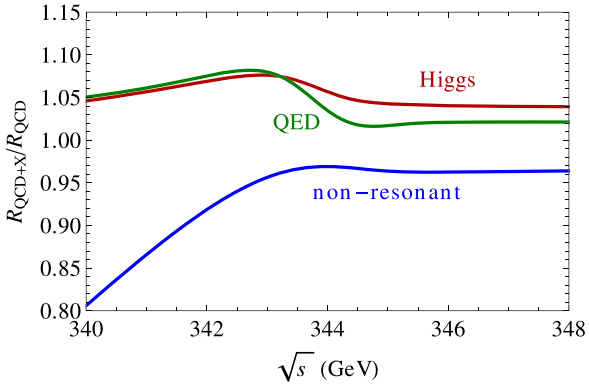


Fig. 3. The sum of the QCD and individual non-QCD contributions to the $R$ ratio, normalized to the QCD-only result, as functions of the center-of-mass energy.

(always $\mu = 80$ GeV). The peak of the QCD-only cross section for the adopted parameters is at $\sqrt{s} = 343.95$ GeV (see Fig. 4). The Higgs and QED contributions result in positive shifts of the cross section of about 4–8% for the former and 2–8% for the latter, depending on the value of $\sqrt{s}$. Both shift the peak to lower energies, thus resulting in larger enhancements below the peak of the QCD-only result. The NLO non-resonant correction is a nearly energy-independent, negative contribution [9] in absolute size and is therefore increasingly important below threshold, which explains the shape of the corresponding line in Fig. 3. Its absolute size is smaller than the sum of the QED and Higgs contributions in the peak region and above, which leads to the overall positive shift in these regions observed in Fig. 2. Below threshold the resonant contribution falls off quickly and the relative correction from the non-resonant part becomes very large, up to 20%. The same behavior is found for the dependence on the scale $\mu_w$. For variations in physically reasonable ranges from the potential to the hard scale we find a relative uncertainty of less than $\pm 1\%$ above threshold, but up to $\pm 3\%$ a few GeV below threshold. The dominant part of this uncertainty comes from the NNLO corrections and cancels exactly once the NNLO non-resonant corrections are included, after which the remaining $\mu_w$ dependence is at most 1%. We note the uncertainty from $\mu_w$ variation is not included in Fig. 2 and subsequent figures that show scale variations.

For a determination of the top-quark mass from the threshold cross section, the sharp rise and the peak in the cross section are its most important features. On the other hand, determinations of the top-quark decay width and its Yukawa coupling require a precise knowledge of the overall normalization. In order to judge the influence of the Higgs, QED, and non-resonant contribution on these quantities, Fig. 4 shows the impact on the peak (upper plot) and maximal slope (lower plot) of the cross section, when these contributions are added successively to the QCD-only result. The theoretical uncertainty due to the variation of $\alpha_s(M_Z)$ within its uncertainty given in (4.2) is shown as the inner error bars. The outer error bars are the quadratic sum of the $\alpha_s$ and scale uncertainty. They provide an indication of the significance of the changes.

The Higgs and QED contributions result in a negative shift of the peak position and an increase in the peak height. Correspondingly, the position of the maximal slope is also shifted to a lower energy and its value is increased when these contributions are added to the QCD result. The Higgs contribution shifts the peak position by $-35$ MeV and the QED contributions adds another $-71$ MeV. Since the peak position is related to twice the top-quark mass, this translates into a

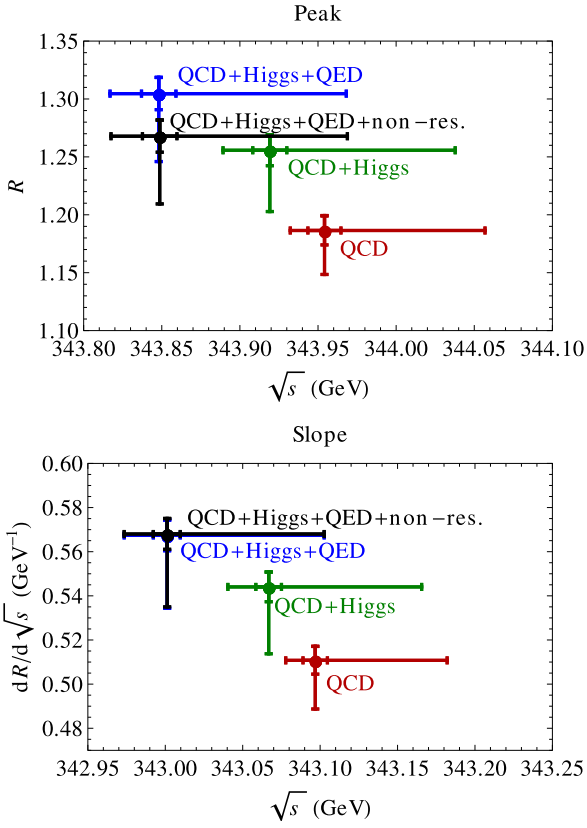


Fig. 4. The upper plot shows the peak height versus the peak position of the $R$ ratio for QCD-only (red), QCD+Higgs (green), QCD+Higgs+QED (blue) and including all contributions (black). The inner error bar denotes the uncertainty due to $\alpha_s(M_Z)$, while the outer one denotes the quadratic sum of the scale and $\alpha_s$ uncertainties. The lower plot is the same but for the maximal slope. In this case there is no visible change due to the non-resonant contribution. (For interpretation of the references to color in this figure legend, the reader is referred to the web version of this article.)

−53 MeV difference in the top-quark masses obtained from the full and QCD-only results for the cross section. Since the non-resonant contribution is an almost energy-independent negative shift, it has almost no influence on the position of the peak and only decreases its height. It also leaves the slope unchanged. Therefore, it is mostly important for the overall normalization of the cross section.

## 5. Sensitivity to the top Yukawa coupling

The mechanism of fermion mass generation in the Standard Model (SM) is intimately related to the question whether the Yukawa coupling of the Higgs boson to fermion $f$ is proportional to the fermion's mass, $y_f = \sqrt{2}m_f/v$. In the SM effective theory including dimension-six operators [25,26] this relation can be violated, for example, by the operator

$$\Delta\mathcal{L} = -\frac{c_{\rm NP}}{\Lambda^2}(\phi^\dagger\phi)(\bar{Q}_3\widetilde{\phi}t_R) + \text{h.c.}, \tag{5.1}$$

where $c_{\rm NP}$ is a new, independent coupling, $\Lambda$ the scale of new physics and $\widetilde{\phi} = i\sigma^2\phi^*$. For simplicity we have neglected flavor indices and assume the new physics to only affect the third generation. After spontaneous symmetry breaking, the operator generates corrections to the top mass term and Higgs coupling,

$$\Delta\mathcal{L} \supset -\frac{c_{\rm NP} v^2}{2\sqrt{2}\Lambda^2}\left(v\bar{t}_L t_R + 3h\bar{t}_L t_R\right) + \text{h.c.}, \tag{5.2}$$

where $h$ denotes the physical Higgs field. We observe that the coefficients of the mass and Yukawa term differ, and obtain the relation

$$\kappa_t \equiv \frac{y_t}{\sqrt{2}m_t/v} = 1 + \frac{c_{\rm NP}}{\Lambda^2}\frac{v^3}{\sqrt{2}m_t}, \tag{5.3}$$

where

$$m_t = \frac{v}{\sqrt{2}}\left(y_t^{\rm SM} + \frac{c_{\rm NP} v^2}{2\Lambda^2}\right) \quad \text{and} \quad y_t = y_t^{\rm SM} + \frac{3c_{\rm NP} v^2}{2\Lambda^2}. \tag{5.4}$$

Below we will use $\kappa_t$ defined in (5.3) to parametrize corrections to the standard relation between $y_t$ and $m_t$. To investigate the sensitivity of the top anti-top cross section to $\kappa_t$, we do not use the SM relation between $m_t$ and $y_t$ in the calculation of the Higgs contribution, and rescale $y_t$ by $\kappa_t$ in the Higgs potential (2.2) and the short-distance contributions. That is, we simply assume that some new physics effect makes the top mass and Yukawa coupling independent parameters. Evidently, the complete set of dimension-six operators may induce further anomalous couplings of the top quark, such as an anomalous top–gluon coupling, which can give additional short-distance and potential contributions to the cross section. A full treatment of these effects is beyond the scope of this work.

The sensitivity of the $R$ ratio to variations of the Yukawa coupling is shown in the upper plot of Fig. 5. The plot shows curves for different values of $\kappa_t$ normalized to the result at $\kappa_t = 1$ and $\mu = 80$ GeV. The main effect of an increase (decrease) in the Yukawa coupling is a strengthening (weakening) of the attractive potential between the top and anti-top quarks. This results in an increase of the cross section of 5–10% for $\kappa_t = 1.5$ or a decrease of 3–5% for $\kappa_t = 0.5$, with some dependence on the center-of-mass energy. In order to provide a first estimate of the possible precision of a Yukawa coupling measurement from top anti-top threshold production, the plot also shows the theoretical uncertainty due to the variation of the renormalization scale $\mu$. Naively one would expect to be only sensitive to values of the Yukawa coupling that lie outside this uncertainty band. From the figure we see that this requires rather large deviations from the SM value of roughly $+20\%$ or $-50\%$. However, a more detailed analysis should also take into account the shape of the curve, which may lead to an improved sensitivity.

Another important point is that a variation of the strong coupling leads to similar changes in the cross section as a variation of the Yukawa coupling. This can be seen by comparing the upper and lower plot in Fig. 5, where the lower one shows curves for $\alpha_s(M_Z) = 0.1205$ and $\alpha_s(M_Z) = 0.1165$. Just as for the Yukawa coupling, an increase (decrease) of the strong coupling leads to an increased (decreased) cross section, though the energy dependence of the shift is slightly different. To make this point clearer, Fig. 6 shows the change in height and position of the peak of the $R$ ratio due to changes in the strong and Yukawa coupling. The similar slope of the resulting lines indicates the degeneracy in the variations of the two parameters. Thus, the precision of a Yukawa coupling measurement depends on the uncertainty of $\alpha_s(M_Z)$. Alternatively, one could

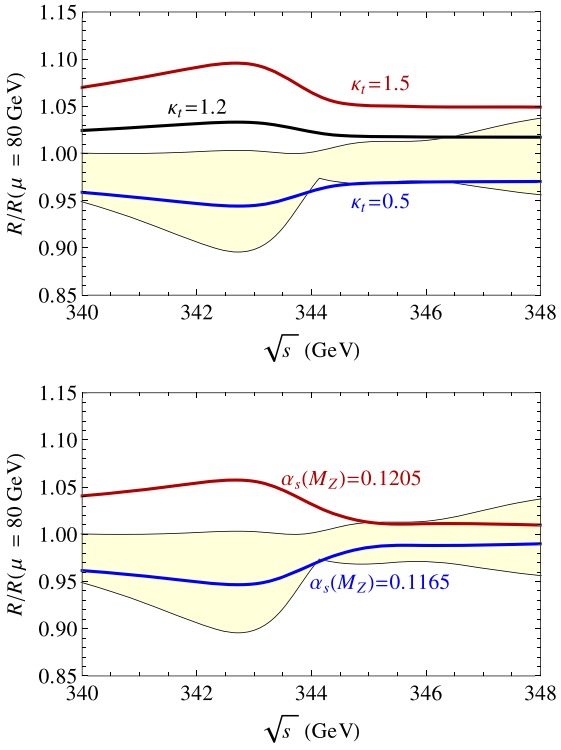


Fig. 5. The sensitivity of the $R$ ratio to the variation of the Yukawa coupling (upper plot) and the strong coupling (lower plot). The bands denote the uncertainty due to scale variation of the $R$ ratio for $y_t = y_t^{\rm SM}$ ($\kappa_t = 1$) and $\alpha_s(M_Z) = 0.1185$. All values have been normalized to the $R$ ratio evaluated at $\mu = 80$ GeV.

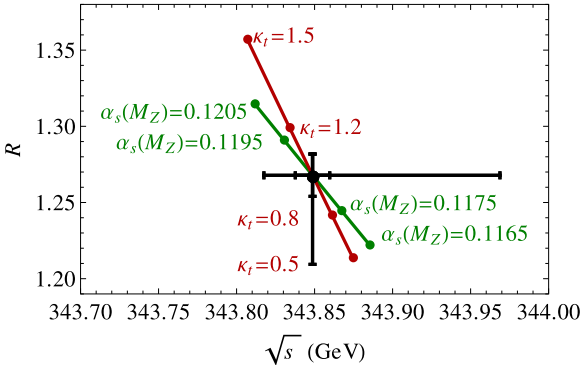


Fig. 6. Changes in peak height and position due to variation of the Yukawa coupling (red line) and the strong coupling (green line). The black error bars denote the $\alpha_s$ and combined scale and $\alpha_s$ uncertainty for $y_t = y_t^{\rm SM}$ ($\kappa_t = 1$) and $\alpha_s(M_Z) = 0.1185$ (cf. upper plot in Fig. 4). (For interpretation of the references to color in this figure legend, the reader is referred to the web version of this article.)

perform a simultaneous fit of both couplings, though this would again lead to a loss in precision for the Yukawa coupling.

Ref. [27] finds that for a Higgs boson with a mass of about 125 GeV the top quark Yukawa coupling can be obtained with a statistical uncertainty of only 4.2%. This result is based on the

increase of the cross section from $y_t = 0$ to $y_t = y_t^{\rm SM}$, which is assumed to be 9% and energy independent. Neither the theoretical uncertainty of the cross section, nor the correlation with the strong coupling constant is considered. Our results show that once theoretical uncertainties are taken into account, it is unlikely that such a high precision can be achieved.

## 6. Conclusion

The completion of the NNNLO QCD correction to the top anti-top production cross section near threshold has increased the precision of the theoretical prediction to a level where non-QCD effects gain importance. In this paper we added NNNLO Higgs, and the leading (NLO) QED and non-resonant contributions to the third-order QCD result for the top anti-top production cross section. All three effects are larger than the current QCD uncertainty of about $\pm 3\%$ [3] and cause a distinct modification of the cross section below, near and above the peak. We quantified the theoretical uncertainty in the presence of these effects, the dependence on the strong coupling, and the sensitivity to a modification of the top–Yukawa coupling. Further studies should be performed in the framework of realistic simulations accounting for beam and initial-state radiation effects. On the theoretical side, the inclusion of NNLO electroweak and non-resonant corrections would further sharpen the prediction, especially below the resonance peak.

## Acknowledgements

We thank Y. Kiyo and P. Ruiz-Femenía for comments, and M. Steinhauser for comments and helpful communications about Ref. [7]. This work was supported by the Gottfried Wilhelm Leibniz programme of the Deutsche Forschungsgemeinschaft (DFG) and the DFG cluster of excellence "Origin and Structure of the Universe".

## Appendix A. Higgs contribution to the hard matching coefficient

For convenience we give the expressions used for the Higgs contribution to the hard matching coefficient of the vector current (2.4). The results are taken from [7], only the prefactors have been adjusted to match our convention.

$$c_{vH}^{(2)} = \frac{1}{\pi^2}\left[\frac{3z-1}{12z} - \frac{2-9z+12z^2}{48z^2}\ln z + \frac{2-5z+6z^2}{24z}\Psi(z)\right], \tag{A.1}$$

where $z = m_t^2/m_H^2$ and

$$\Psi(z) = \begin{cases} \dfrac{\sqrt{4z-1}}{z}\arctan\sqrt{4z-1}, & z \geq 1/4, \\ \dfrac{\sqrt{1-4z}}{2z}\ln\dfrac{1-\sqrt{1-4z}}{1+\sqrt{1-4z}}, & z < 1/4. \end{cases} \tag{A.2}$$

$$c_{vH}^{(3)} = \frac{4C_F}{\pi^2}\left[\frac{\pi^2}{8}(1-y)\ln\frac{m_t^2}{\mu^2} - 5.760 + 5.533y - 0.171y^2 + 0.0124y^3 + 0.0304y^4 + 0.0296y^5 + \ldots\right], \tag{A.3}$$

where $y = 1 - z$.

## References


[1] M. Beneke, A. Signer, V.A. Smirnov, Top quark production near threshold and the top quark mass, Phys. Lett. B 454 (1999) 137–146, arXiv:hep-ph/9903260.

[2] A.H. Hoang, et al., Top–antitop pair production close to threshold: synopsis of recent NNLO results, Eur. Phys. J. direct C 2 (2000) 1, arXiv:hep-ph/0001286.

[3] M. Beneke, Y. Kiyo, P. Marquard, A. Penin, J. Piclum, M. Steinhauser, Next-to-next-to-next-to-leading order QCD prediction for the top anti-top S-wave pair production cross section near threshold in $e^+e^-$ annihilation, arXiv:1506.06864.

[4] M.J. Strassler, M.E. Peskin, The heavy top quark threshold: QCD and the Higgs, Phys. Rev. D 43 (1991) 1500–1514.

[5] R.J. Guth, J.H. Kühn, Top quark threshold and radiative corrections, Nucl. Phys. B 368 (1992) 38–56.

[6] R. Harlander, M. Jeżabek, J.H. Kühn, Higgs effects in top quark pair production, Acta Phys. Pol. B 27 (1996) 1781, arXiv:hep-ph/9506292.

[7] D. Eiras, M. Steinhauser, Complete Higgs mass dependence of top quark pair threshold production to order $\alpha\alpha_s$, Nucl. Phys. B 757 (2006) 197–210, arXiv:hep-ph/0605227.

[8] M. Beneke, J. Piclum, T. Rauh, P-wave contribution to third-order top-quark pair production near threshold, Nucl. Phys. B 880 (2014) 414–434, arXiv:1312.4792.

[9] M. Beneke, B. Jantzen, P. Ruiz-Femenía, Electroweak non-resonant NLO corrections to $e^+e^- \to W^+W^-b\bar{b}$ in the $t\bar{t}$ resonance region, Nucl. Phys. B 840 (2010) 186–213, arXiv:1004.2188.

[10] A.A. Penin, J.H. Piclum, Threshold production of unstable top, J. High Energy Phys. 1201 (2012) 034, arXiv:1110.1970.

[11] M. Beneke, Y. Kiyo, K. Schuller, Third-order correction to top-quark pair production near threshold I. Effective theory set-up and matching coefficients, arXiv:1312.4791.

[12] B. Grzadkowski, J.H. Kühn, P. Krawczyk, R. Stuart, Electroweak corrections on the toponium resonance, Nucl. Phys. B 281 (1987) 18.

[13] A.H. Hoang, C.J. Reißer, On electroweak matching conditions for top pair production at threshold, Phys. Rev. D 74 (2006) 034002, arXiv:hep-ph/0604104.

[14] P. Marquard, J.H. Piclum, D. Seidel, M. Steinhauser, Three-loop matching of the vector current, Phys. Rev. D 89 (3) (2014) 034027, arXiv:1401.3004.

[15] M. Beneke, A.P. Chapovsky, A. Signer, G. Zanderighi, Effective theory approach to unstable particle production, Phys. Rev. Lett. 93 (2004) 011602, arXiv:hep-ph/0312331.

[16] M. Beneke, A.P. Chapovsky, A. Signer, G. Zanderighi, Effective theory calculation of resonant high-energy scattering, Nucl. Phys. B 686 (2004) 205–247, arXiv:hep-ph/0401002.

[17] B. Jantzen, P. Ruiz-Femenía, NNLO non-resonant corrections to threshold top-pair production from $e^+e^-$ collisions: endpoint-singular terms, Phys. Rev. D 88 (2013) 054011, arXiv:1307.4337.

[18] P. Ruiz-Femenía, First estimate of the NNLO nonresonant corrections to top–antitop threshold production at lepton colliders, Phys. Rev. D 89 (2014) 097501, arXiv:1402.1123.

[19] M. Beneke, Y. Kiyo, K. Schuller, Third-order Coulomb corrections to the S-wave Green function, energy levels and wave functions at the origin, Nucl. Phys. B 714 (2005) 67, arXiv:hep-ph/0501289.

[20] M. Beneke, Y. Kiyo, K. Schuller, Third-order correction to top-quark pair production near threshold II. Potential contributions, to be published.

[21] A. Pineda, A. Signer, Heavy quark pair production near threshold with potential non-relativistic QCD, Nucl. Phys. B 762 (2007) 67–94, arXiv:hep-ph/0607239.

[22] A.H. Hoang, C.J. Reißer, P. Ruiz-Femenía, Phase space matching and finite lifetime effects for top-pair production close to threshold, Phys. Rev. D 82 (2010) 014005, arXiv:1002.3223.

[23] M. Beneke, A quark mass definition adequate for threshold problems, Phys. Lett. B 434 (1998) 115–125, arXiv:hep-ph/9804241.

[24] K. Hagiwara, R. Liao, A.D. Martin, D. Nomura, T. Teubner, $(g-2)_\mu$ and $\alpha(M_Z^2)$ re-evaluated using new precise data, J. Phys. G 38 (2011) 085003, arXiv:1105.3149.

[25] W. Buchmüller, D. Wyler, Effective Lagrangian analysis of new interactions and flavor conservation, Nucl. Phys. B 268 (1986) 621–653.

[26] B. Grzadkowski, M. Iskrzynski, M. Misiak, J. Rosiek, Dimension-six terms in the standard model Lagrangian, J. High Energy Phys. 1010 (2010) 085, arXiv:1008.4884.

[27] T. Horiguchi, A. Ishikawa, T. Suehara, K. Fujii, Y. Sumino, et al., Study of top quark pair production near threshold at the ILC, arXiv:1310.0563.